Article

Chromatin remodeler CHD4 establishes chromatin states required for ovarian reserve formation, maintenance, and germ cell survival

Yasuhisa Munakata[1], Mengwen Hu[1], Yuka Kitamura[1], Adam L. Bynder[1], Amelia S. Fritz[1], Richard M. Schultz[1,2]*, Satoshi H. Namekawa[1]*

[1] Department of Microbiology and Molecular Genetics, University of California, Davis, CA 95616, USA

[2] Department of Biology, University of Pennsylvania, Philadelphia, PA 19104, USA

*Correspondence: snamekawa@ucdavis.edu, rschultz@sas.upenn.edu

13   **Abstract**

14   The ovarian reserve defines female reproductive lifespan, which in humans spans decades due to the

15   maintenance of meiotic arrest in non-growing oocytes (NGO) residing in primordial follicles. Unknown is

16   how the chromatin state of NGOs is established to enable long-term maintenance of the ovarian reserve.

17   Here, we show that a chromatin remodeler, CHD4, a member of the Nucleosome Remodeling and

18   Deacetylase (NuRD) complex, establishes chromatin states required for formation and maintenance of the

19   ovarian reserve. Conditional loss of CHD4 in perinatal mouse oocytes results in acute death of NGOs and

20   depletion of the ovarian reserve. CHD4 establishes closed chromatin at regulatory elements of pro-

21   apoptotic genes to prevent cell death and at specific genes required for meiotic prophase I to facilitate the

22   transition from meiotic prophase I oocytes to meiotic arrested NGOs. In addition, CHD4 establishes

23   closed chromatin at the regulatory elements of pro-apoptotic genes in male germ cells, allowing male

24   germ cell survival. These results demonstrate a role for CHD4 in defining a chromatin state that ensures

25   germ cell survival, thereby enabling the long-term maintenance of both female and male germ cells.

Introduction

Germ cell maintenance and survival are fundamental for the continuous supply of gametes for reproduction. In adult mammals, while the male germline is maintained by self-renewal of spermatogonial stem cells, the female germline is not maintained by a stem cell-based mechanism but is maintained within a pool of meiotically arrested oocytes, called the ovarian reserve. These small non-growing oocytes (NGOs) residing in primordial follicles are arrested at the dictyate stage, the prolonged diplotene stage, of meiotic prophase I (MPI) [1]. NGOs are the only source of fertilizable eggs throughout a female's reproductive life span. Because the number of NGOs is finite, their premature depletion leads to infertility associated with early menopause, such as premature ovarian insufficiency (POI)[2]. However, the mechanisms underlying formation and maintenance of the ovarian reserve remain largely elusive.

In the female germline of mouse embryos, primordial germ cells (PGCs) initiate MPI after induction of genes specifically expressed in MPI (MPI genes)[3]. After completing chromosome synapsis and recombination, oocytes reach the dictyate stage around birth, gradually decreasing in number before formation of the ovarian reserve [4, 5, 6]. During ovarian reserve formation, MPI genes are suppressed, and there is a transition in genome-wide transcription to become NGOs, which is termed the perinatal oocyte transition (POT)[7, 8]. POT is regulated by an epigenetic regulator, Polycomb Repressive Complex 1 (PRC1), to suppress MPI genes when oocytes exit MPI[7]. Concomitantly, an oocyte-specific transcription factor FIGLA and several signaling pathways, such as Notch, TGF-β, JNK, and hypoxia signaling that regulate gene expression are required for primordial follicle formation[9, 10, 11, 12, 13]. These studies raise the possibility that the chromatin state in NGOs is uniquely established to instruct the gene expression program for ovarian reserve formation.

To identify a chromatin-based mechanism underlying the process of the ovarian reserve formation and maintenance, we sought to examine the role of ATP-dependent chromatin remodelers that utilize the energy from ATP hydrolysis to reorganize chromatin and regulate gene expression[14, 15]. There are four major subfamilies of chromatin remodeling complexes, including SWI/SNF (switch/sucrose non-fermentable), ISWI (imitation SWI), NuRD (nucleosome remodeling and deacetylase)/CHD (chromodomain helicase DNA-binding)/mi-2, and INO80/SWR (SWI2/SNF2 related) families[14, 15]. Among the ATPase subunits in these four major chromatin remodeler subfamilies, we focused our attention on CHD4 (also known as Mi-2β) based on its gene expression at POT and because CHD4 is associated with lineage commitment and differentiation processes[16, 17, 18, 19]. In the male germline, CHD4 regulates maintenance and survival of undifferentiated spermatogonia[20, 21, 22]. However, the molecular mechanisms underlying this process remain unknown.

60   Here we show that CHD4 has an essential function in formation and maintenance of the ovarian reserve

61   and determine the molecular mechanisms common to both female and male germ cells. In the female

62   germline, CHD4 establishes closed chromatin at regulatory elements of pro-apoptotic genes to prevent

63   cell death and at MPI genes to facilitate the transition from MPI to NGO. Further, in the male germline,

64   CHD4 establishes closed chromatin at the regulatory elements of pro-apoptotic genes, allowing male

65   germ cell survival. Thus, CHD4 defines the chromatin state for maintenance of both female and male

66   germ cells.

67

68   **Results**

69   **CHD4 is required for ovarian reserve formation**

70   To identify a key ATP-dependent chromatin remodeler that functions in ovarian reserve formation in

71   mice, we compared gene expression profiles of ATPase subunits in representative chromatin remodeler

72   subfamilies using previously published RNA-seq data[13]. Among these candidates, *Chd4* is highly

73   expressed from embryonic day 14 (E14.5) oocytes in MPI to postnatal day 4 (P4) and P6 NGOs, which

74   corresponds to the time of ovarian reserve formation when genome-wide gene expression changes occur

75   during POT[7] (Fig. 1a). *Chd4* expression was slightly downregulated when NGOs in primordial follicle

76   (labeled as "small" in Fig. 1a) are activated to become growing oocytes (GOs) in primary follicles

77   (labeled as "large" in Fig. 1a); this transition is termed the primordial to primary follicle transition

78   (PPT)[13], and the first wave occurs as early as P4 (Fig. 1a). Based on this gene expression profile, we

79   focused on CHD4 and sought to determine the function of CHD4 in ovarian reserve formation.

80

81   To determine the function of CHD4 in ovarian reserve formation, we generated *Chd4* conditional

82   knockout mice using the *Chd4* floxed allele[23] and *Ddx4*-Cre transgene, which is a germline-specific Cre

83   line expressed from E15.5[24] (*Chd4* [f/-]; *Ddx4*-Cre [Tg/+]; termed *Chd4* DcKO, Fig. 1b). CHD4 protein

84   localized in the nucleus of the P1 oocytes in littermate controls (*Chd4* [f/+]; *Ddx4*-Cre [Tg/+]; termed *Chd4*

85   Dctrl), but was absent in 98.8% of the P1 oocyte nuclei of *Chd4* DcKO mice (Fig1c, d), confirming the

86   efficient deletion of CHD4 protein in *Chd4* DcKO oocytes. The estimated oocyte number of *Chd4* DcKO

87   neonatal mice at P1 did not differ from that of *Chd4* Dctrl (Fig. 1e, f). However, by P5, when the ovarian

88   reserve is established, the estimated oocyte number of *Chd4* DcKO newborn mice was markedly reduced

89   compared to *Chd4* Dctrl (Fig. 1e, f). Apoptosis was likely responsible for the loss of oocytes in *Chd4*

90   DcKO newborn mice because immunofluorescence staining for cleaved Caspase 3, a marker of apoptosis,

91   revealed no difference in the proportion of cleaved Caspase 3-positive oocytes in P1, whereas the

92   proportion of cleaved Caspase 3-positive oocytes in P3 *Chd4* DcKO ovaries was significantly increased

93   compared to *Chd4* Dctrl (Fig. 2a, b). These results suggest that CHD4 is critical for ovarian reserve

94   formation.

95

96   We next examined whether the ovarian reserve is properly established in *Chd4* DcKO ovaries. During the

97   formation of NGOs in the ovarian reserve, localization of the transcription factor FOXO3 changes from

98   the cytoplasm to the nucleu[25]; nuclear localization of FOXO3 is a hallmark of NGOs[25].

99   Immunofluorescence staining for FOXO3 showed that in P1 FOXO3 was localized in the cytoplasm of

100   most oocytes in both *Chd4* Dctrl and *Chd4* DcKO (Fig. 2c, d). However, at P3, FOXO3 was localized in

101   the nucleus of 92.9% of oocytes in *Chd4* Dctrl whereas nuclear localization was only 7.9% of oocytes in

102   *Chd4* DcKO had FOXO3 (Fig. 2c, d). Therefore, NGOs are not properly generated in *Chd4* DcKO

103   ovaries. Nevertheless, the behavior of meiotic chromosomes in MPI, including progression to the dictyate

104   stage of MPI, appeared normal in *Chd4* DcKO (Supplementary Fig. 1a). Thus, cell death is not initiated

105   by defects in meiotic chromosome behavior.

106

107   **CHD4 represses MPI genes and apoptosis genes in ovarian reserve formation.**

108   To further examine the function of CHD4 in ovarian reserve formation, NGOs were isolated from P1 and

109   P5 ovaries, and RNA-seq analysis was performed (Supplementary Fig. 1b). In P1 *Chd4* DcKO NGOs,

110   533 genes were up-regulated, and 348 genes were down-regulated (Fig. 3a, left, Supplementary Data 1).

111   In P5 *Chd4* DcKO NGOs, 569 genes were up-regulated, and 396 genes were down-regulated (Fig. 3a,

112   right, Supplementary Data 2). To infer possible functions of these differentially expressed genes, we

113   performed Gene ontology enrichment analyses. The genes down-regulated in P1 and P5 *Chd4* DcKO

114   oocytes were enriched with genes involved in "oogenesis" and "female gamete generation". On the other

115   hand, the genes up-regulated in P5 *Chd4* DcKO oocytes were enriched with genes involved in MPI, such

116   as "homologous chromosome pairing at meiosis" (Fig. 3b), suggesting that CHD4 represses MPI genes.

117   During ovarian reserve formation, MPI genes are repressed as oocytes exit from MPI and the fetal

118   program[7]. Therefore, we examined how MPI genes are regulated in *Chd4* DcKO NGOs.

119

120   In a previous study[26], 104 genes were identified to be MPI-specific genes in fetal oocytes[26]. The

121   expression of these MPI genes is comparable between *Chd4* DcKO and *Chd4* Dctrl NGOs at P1 (Fig. 3c).

122   In contrast, in P5 NGOs, expression of MPI genes was significantly up-regulated in *Chd4* DcKO relative

123   to *Chd4* Dctrl (Fig. 3c). Among them, 23 MPI genes, such as *Spo11*[27, 28], *Sycp1*[29], *Hormad1*[30, 31, 32],

124   *Meiob*[33], and *Majin*[34], which are important for MPI progression, were included in the differentially

125   expressed genes in P5 NGOs (Fig. 3d). Because there is a genome-wide gene expression change in POT

126   in normal oogenesis[7], we next examined how differentially expressed genes at POT are regulated in the

127   *Chd4* DcKO NGOs. In P5 *Chd4* DcKO NGOs, up-regulated genes at POT were down-regulated, while

128   down-regulated genes at POT were up-regulated (Supplementary Fig. S1c, d, Supplementary Data 3),

129   further confirming that POT is defective in accordance with defective ovarian reserve formation.

130

131   We also examined the expression of the genes in the mouse apoptosis pathway defined in the KEGG

132   database[35]. Both in P1 and P5 NGOs, *Casp7*, a gene important for apoptosis, was significantly up-

133   regulated (Fig. 3e). Taken together, CHD4 is required for the repression of MPI genes and apoptosis

134   genes during ovarian reserve formation.

135

136   **CHD4 represses chromatin accessibility to down-regulate genes.**

137   Because CHD4 represses transcription and chromatin accessibility in various cell types[16, 36, 37], we next

138   sought to determine how CHD4 regulates chromatin accessibility during ovarian reserve formation. We

139   used the assay for transposase-accessible chromatin by sequencing (ATAC-seq)[38, 39] to assess the effect of

140   CHD4 loss on chromatin accessibility in ovarian reserve formation (Supplementary Fig. 2a). A

141   representative track view confirms that peak patterns are consistent between two biological replicates

142   (Supplementary Fig. 2b). An ATAC-seq analysis of P1 NGOs showed that accessibility was massively

143   increased in *Chd4* DcKO (Fig. 4a). These increased accessibility regions are mainly introns and intergenic

144   regions, and a relatively minor change was observed at promoters and transcription termination sites

145   (TTSs: Fig. 4b). This result suggests that CHD4 regulates distal cis-regulatory elements such as

146   enhancers.

147

148   Next, we examined the relationship between changes in the distal accessible regions and changes in gene

149   expression following CHD4 loss. Expression of 2,906 genes adjacent to *Chd4* Dctrl-specific distal

150   accessible regions (outside the transcription start sites (TSSs) ±1 kb window) was similar between *Chd4*

151   DcKO and *Chd4* Dctrl NGOs both in P1 and P5 (Fig. 4c). However, expression of 5,423 genes adjacent

152   to *Chd4* DcKO-specific distal accessible regions was globally up-regulated in *Chd4* DcKO NGOs both in

153   P1 and P5 (Fig. 4d). Therefore, CHD4 represses distal accessible regions to down-regulate genes. Further,

154   we examined chromatin accessibility at the promoters of differentially expressed genes in *Chd4* DcKO

155   NGOs. We found that up-regulated genes in *Chd4* DcKO NGOs are associated with increased

156   accessibility at promoters both in P1 and P5, whereas down-regulated genes were not associated with

157   changes in chromatin accessibility (Fig. 4e-h). Chromatin accessibility was increased at the TSS of genes

158   whose expression was up-regulated in *Chd4* DcKO; for example, an apoptotic gene *Casp7*, and an MPI

159   gene *Stra8*, which is the transcription factor critical for MPI gene expression[40] (Fig. 4i). Together, we

160 conclude that CHD4 represses chromatin accessibility both at promoters and distal regulatory elements to

161 repress genes in ovarian reserve formation.

162

163 **CHD4 binds chromatin to regulate MPI and apoptosis genes.**

164 Because CHD4 deficiency causes a massive increase in chromatin accessibility, we hypothesize that

165 CHD4 directly binds target sites to regulate chromatin accessibility. To test this hypothesis, we performed

166 Cleavage Under Targets and Tagmentation (CUT&Tag) analysis[41] on CHD4 using P1 oocytes to

167 determine where CHD4 is bound in the genome (Supplementary Fig. 2c). CUT&Tag analysis revealed

168 that the majority of CHD4 peaks were enriched in introns and intergenic regions (Fig. 5a). In addition,

169 most of the CHD4 peaks were located 5-500 kb away from the TSSs (Fig. 5b), consistent with the

170 genomic sites of accessibility changes in *Chd4* DcKO NGOs. We compared the ATAC peaks with the

171 CHD4 peaks and found that, surprisingly, only a minor portion of them overlapped (Supplementary Fig.

172 2d), and this is the case for the ATAC distal peaks (Fig. 5c). We compared the adjacent gene expression

173 near the CHD4 peaks and found that it was significantly increased in P5 *Chd4* DcKO (Fig. 5d),

174 suggesting that CHD4 binds to repress target genes. However, counterintuitively, the CHD4 signals were

175 enriched at the TSSs of the gene that was significantly down-regulated in P1 and P5 *Chd4* DcKO (Fig.

176 5e). These results suggest that CHD4 not only directly regulates chromatin accessibility but may also

177 regulate gene expression without changing chromatin accessibility.

178

179 To further elucidate the function of CHD4 in formation of ovarian reserve, we focused on apoptosis-

180 associated genes and MPI genes whose expression was up-regulated in *Chd4* DcKO NGOs. CHD4 was

181 enriched in the TSSs of the respective gene groups compared to randomly selected regions (Fig. 5f, g). At

182 the *Stra8* gene locus, CHD4 binds the TSS, where chromatin accessibly increased in the *Chd4* DcKO

183 NGOs (Fig. 5h, left). Furthermore, at the pro-apoptotic *Bbc3* (also known as *Puma*) gene locus, CHD4

184 bound not only at the TSS but also at the upstream region where chromatin accessibility was increased in

185 *Chd4* DcKO NGOs (Fig. 5h, right). Thus, for some important target genes, CHD4 directly regulates

186 chromatin accessibility, supporting a model in which CHD4 represses expression by regulating chromatin

187 accessibility.

188

189 **CHD4 is required for the maintenance of the ovarian reserve and oocyte survival.**

190 Because a critical aspect of ovarian reserve is the long maintenance of chromatin states during the female

191 reproductive life span, we next determined whether CHD4 is required for maintenance of ovarian reserve

192 after its establishment. To elucidate the function of CHD4 in the maintenance of NGOs in the ovarian

193 reserve, we generated another line of CHD4 conditional knockout mice using *Gdf9*-iCre, which is

194   expressed NGOs from P3[42] (*Chd4* [f/f]; *Gdf9*-iCre [Tg/+]; termed *Chd4* GcKO) (Fig. 6a). CHD4 was localized

195   in the nuclei of NGOs in primordial follicles and GOs in primary follicles of P10 ovaries, and nearly

196   complete depletion of CHD4 was observed in P10 *Chd4* GcKO oocytes (Supplementary Fig. 3a, b). In

197   P10 ovaries in which primordial follicle formation is complete, the estimated numbers of NGOs and GOs

198   in the ovaries of *Chd4* GcKO mice were significantly reduced in both NGOs and GOs compared to *Chd4*

199   Gctrl mice (Fig. 6b, c). These results indicate that CHD4 is essential for the maintenance of NGOs and

200   the survival of GOs.

201

202   To determine the function of CHD4 in maintenance of ovarian reserve and survival of GOs, NGOs and

203   GOs were isolated from P10 ovaries, and RNA-seq analysis was performed (Supplementary Fig. 3c). In

204   the P10 *Chd4* GcKO NGOs, 947 genes were up-regulated, and 744 genes were downregulated (Fig. 6d,

205   left, Supplementary Data 4). In the P10 *Chd4* GcKO GOs, 1,938 genes were up-regulated, and 1,420

206   genes were down-regulated (Fig. 6d, right, Supplementary Data 4). Gene ontology enrichment analyses

207   show that up-regulated genes in P10 *Chd4* GcKO NGOs were associated with apoptotic cell clearance

208   (Supplementary Fig. 3d). In addition, up-regulated genes in P10 *Chd4* GcKO GOs were enriched with

209   genes involved in synaptonemal complex assembly, which is related to MPI (Supplementary Fig. 3d).

210   Female MPI-specific genes were up-regulated in *Chd4* GcKO GOs (Fig. 6e). Similar to *Chd4* DcKO,

211   *Stra8* expression was increased in both P10 NGOs and GOs in *Chd4* GcKO (Fig. 6f). We also examined

212   apoptosis-related genes and found that the expression of a pro-apoptotic gene, *Bid* [43], a key player in

213   apoptosis, was increased in both NGOs and GOs in *Chd4* GcKO (Fig. 6f). In summary, CHD4 is essential

214   for oocyte survival and maintenance of ovarian reserve by repressing a group of the MPI genes and

215   apoptosis genes.

216

217   **CHD4 repressed apoptosis-related genes for male germ cell survival.**

218   After determining the function of CHD4 in the female germline, we finally sought to address whether

219   CHD4 has a common function in the female and male germline. In the male germline, around the time of

220   birth, mitotically arrested prospermatogonia resume active cell cycle and transition to spermatogonia after

221   birth, which sustains long-term fertility of males by stem self-renewal[44]. Recent studies using germline-

222   specific conditional knockout of CHD4 revealed that CHD4 is required for the survival of

223   undifferentiated spermatogonia[20, 21]. Consistent with these studies, our *Chd4* DcKO males (Fig. 7a)

224   showed germ cell depletion that became evident at P3 testes (Fig. 7b).

225

226   To examine the genes regulated by CHD4, we isolated undifferentiated male germ cells from P3 testes

227   using a previously established fluorescence-activated cell sorting (FACS) method [45, 46] and performed

228   RNA-seq analysis (Supplementary Fig. 4a). In P3 *Chd4* DcKO male germ cells, 696 genes were up-

229   regulated, and 168 genes were down-regulated (Fig. 7c, Supplementary Data 5). Gene ontology

230   enrichment analyses revealed that the genes up-regulated in *Chd4* DcKO male germ cells were associated

231   with "cell morphogenesis" and "regulation of secretion by cell" (Supplementary Fig. 4b). Next, we

232   examined whether the expression of MPI genes is up-regulated by CHD4 deletion, as observed in

233   oocytes, but found no difference in the expression of 104 female MPI genes (Supplementary Fig. 4c).

234   However, a pro-apoptotic gene *Bbc3* and *Gadd45g* were up-regulated in *Chd4* DcKO male germ cells, as

235   was observed in oocytes (Fig. 7d, and Supplementary Fig. 4d). Thus, CHD4 represses the *Bbc3* and

236   *Gadd45* genes in both males and females.

237

238   To determine whether CHD4 also represses accessible chromatin in male germ cells, we performed

239   ATAC-seq analysis on P3 *Chd4* DcKO male germ cells (Supplementary Fig. 4e). Chromatin accessibility

240   was increased in *Chd4* DcKO male germ cells compared to P3 *Chd4* Dctrl, as observed in oocytes (Fig.

241   7e). In addition, P3 *Chd4* DcKO male germ cells -specific ATAC peaks were enriched in intron and

242   intergenic regions, and only slightly in the promoter-TSS region (Fig. 7f). As shown in the track view,

243   chromatin accessibility of the *Bbc3* gene at the TSS was increased (Fig. 7d). These results indicate that

244   CHD4 suppresses expression of apoptosis genes by repressing chromatin accessibility in P3 *Chd4* DcKO

245   male germ cells, leading to cell survival. Taken together, we conclude that CHD4 defines the chromatin

246   state to ensure germ cell survival, enabling the long-term maintenance of female and male germ cells.

247

248   **Discussion**

249   The germline must maintain genome integrity to ensure generation of the offspring. Thus, mechanisms

250   underlying long-term maintenance of the germline are critical at sexually dimorphic stages of the

251   germline: one for maintenance of the ovarian reserve in females and another for maintenance of

252   spermatogonial stem cells in males. We report here that CHD4 is a critical regulator for the long-term

253   maintenance of the germline in both males and females. In combination with mouse genetics and

254   epigenomic analyses, our study reveals that CHD4 directly binds and closes accessible chromatin at the

255   distal regulatory elements genome-wide. This mechanism underlies regulation of pro-apoptotic genes in

256   both females and males (Fig. 7g). Notably, the female germline is maintained in the ovarian reserve after

257   MPI and CHD4 is required to close the regulatory elements for MPI genes in females but not in males

258   (Fig. 7g). These results highlight the common and distinct features of chromatin regulation in female and

259   male germlines.

260

261   We find that CHD4 is required for both formation and maintenance of ovarian reserve. Because CHD4

262   has a maintenance function after ovarian reserve formation, it is likely that CHD4 continues to associate

263   with chromatin in MPI-arrested NGOs. The histone H3.3 chaperone HIRA, which continues to replace

264   H3.3 in NGOs is critical to maintain the ovarian reserve[47], suggesting that the chromatin state of NGOs is

265   not so static. Thus, a chromatin remodeler may be required to maintain a dynamic chromatin environment

266   in NGOs. Furthermore, loss of the DNA damage response (DDR) genes has been implicated in ovarian

267   aging, suggesting a possible function of DDR in the ovarian reserve maintenance[48]. Noteworthy is that

268   CHD4 is known to function in the context of DDR[49, 50]. To further clarify the molecular mechanism for

269   CHD4 in formation and maintenance of the ovarian reserve, the composition of the CHD4-containing

270   chromatin remodeling complex needs to be determined to distinguish its function from other chromatin

271   remodelers whose functions are not known in ovarian reserve formation.

272

273   Another critical regulator of POT is PRC1 for MPI exit[7]. Notably, MPI genes repressed by CHD4 (Fig.

274   3d) are also repressed by PRC1[7], suggesting possible coordination between CHD4 and PRC1 in MPI exit.

275   In this context, CHD4 closes the accessible chromatin at POT. Consistent with this observation, in

276   embryonic stem cells, CHD4-containing NuRD complexes deacetylate histone H3K27 and recruit PRC2,

277   which often functions with PRC1 to facilitate H3K27me3-mediated repression[51]. On the other hand,

278   CHD4 was also enriched at downregulated genes in *Chd4* DcKO NGOs at P1 and P5 (Fig. 5e), suggesting

279   the possible function of CHD4 in gene activation. Indeed, CHD4 also functions in gene activation[23],

280   raising the possibility that the function of CHD4 is context-dependent for both gene repression and

281   activation.

282

283   We also investigated the target sites of CHD4 chromatin remodeling. The majority of CHD4 binding sites

284   and the accessible chromatin sites closed by CHD4 are intergenic regions and introns. We examined *de*

285   *novo* motifs present in cKO-specific ATAC peaks (i.e., sites closed by the action of CHD4 in wild-type)

286   in both females and males (Supplementary Fig. 4f). In females, the PRDM9 motif, which is often a

287   feature of meiotic recombination sites, was highly enriched, consistent with CHD4 facilitating exit from

288   the MPI program. The ZNF11 motif was commonly enriched in both females and males, suggesting a

289   common program between males and females. Intriguingly, the NFYB and POU3F1 motifs, detected in

290   males, become open in late spermatogenesis[52]. Thus, it is tempting to speculate that the regulatory

291   elements used in late spermatogenesis are remodeled by CHD4 at an early stage, which may represent a

292   mechanism for epigenetic priming often observed in the male germline[53].

293

294   Together, our study reveals a chromatin remodeling mechanism underlying regulatory elements required

295   for key developmental transitions in the germline. A next key question is how these specific sites are

296   determined to be regulated by CHD4. Because transcription factors (FIGLA, FOXO3) and several

297   signaling pathways (Notch, TGF-β, JNK, and hypoxia signaling) are implicated in primordial follicle

298   formation, it will be important to understand how these mechanisms intersect with chromatin remodeling

299   to establish the necessary chromatin states for ovarian reserve formation. Furthermore, given the

300   significant role of the RNA regulatory network in primordial follicle formation[54], the mechanistic

301   relationship between the RNA regulatory network and chromatin-based cellular memory emerges as an

302   important agenda for future investigation.

303

304   **Methods**

305

306   **Animals**

307   Generation of conditionally deficient *Chd4* DcKO mice, *Chd4 f/-; Ddx4-Cre Tg/+,* were generated from

308   *Chd4 f/f* female crossed with *Chd4 f/+; Ddx4-Cre Tg/+* males, and *Chd4* Dctrl mice used in experiments

309   were *Chd4 f/+; Ddx4-Cre Tg/+* littermate. Generation of conditionally deficient *Chd4* GcKO mice, *Chd4*

310   *f/f; Gdf9-iCre Tg/+,* were generated from *Chd4 f/f* female crossed with *Chd4 f/f; Gdf9-iCre Tg/+* males,

311   and *Chd4* Gctrl mice used in experiments were *Chd4 f/f* littermate. Generation of *Chd4* floxed alleles

312   (*Chd4 f/f*) were reported previously[23]. Mice were maintained on a mixed genetic background of C57BL/6

313   and DBA2. Ddx4-Cre transgenic mice were purchased from the Jackson Laboratory[24]. For ATAC-seq and

314   CUT&Tag, *Chd4 f/f; Stella*-GFP *Tg/+* mice were generated from *Chd4 f/f* mice crossed with *Stella*-GFP

315   *Tg/+* mice. *Stella*-GFP transgenic mice were obtained from Dr. M. Azim Surani[55]. For each experiment, a

316   minimum of three mice was analyzed. Mice were maintained on a 12:12 light: dark cycle in a temperature

317   and humidity-controlled vivarium (22 ± 2 °C; 40–50% humidity) with free access to food and water in

318   the pathogen-free animal care facility. Mice were used according to the guidelines of the Institutional

319   Animal Care and Use Committee (IACUC: protocol no. IACUC 21931 and 23545) at the University of

320   California, Davis.

321

322   **Oocyte collection**

323   The P1, P5, or P10 female pups were collected, and ovaries were harvested by carefully removing

324   oviducts and ovarian bursa in PBS. Ovaries were digested in 200 μl TrypLE™ Express Enzyme (1X)

325   (Gibco, 12604013) supplemented with 0.3 mg/ml Collagenase Type 1 (Worthington, CLS-1) and 10

326   mg/ml DNase I (Sigma, D5025) and incubated at 37°C for 25 min with gentle agitation. After incubation,

327   the ovaries were dissociated by gentle pipetting using the Fisherbrand™ Premium Plus MultiFlex Gel-

328   Loading Tips until no visible tissue pieces. 2 ml DMEM/F-12 medium (Gibco, 11330107) supplemented

329   with 10% FBS (HyClone, SH30396.03) were then added to the suspension to stop enzyme reaction. Cell

330   suspension was seeded onto a 60 mm tissue culture dish (Falcon, 353002). The cells were allowed to

331   settle down for 15 min at 37°C; 5% CO_2 in the incubator before being transferred under the microscope

332   (Nikon, SMZ1270). For RNA-seq, based on morphology and diameter, non-growing and growing oocytes

333   were manually picked up, washed in M2 medium (Sigma, M7167), and transferred into the downstream

334   buffer by mouth pipette. For ATAC-seq and CUT&Tag, P1 non-growing oocytes expressing a *Stella*-GFP

335   transgene were collected by FACS (SONY SH800S).

336

337   **Histology and Immunostaining**

338   For the preparation of paraffin blocks, ovaries, and testis were fixed with 4% paraformaldehyde overnight

339   at 4 °C. Ovaries and testis were dehydrated and embedded in paraffin. For histological analysis, 5 μm-

340   thick paraffin sections were deparaffinized and stained with hematoxylin (Sigma, MHS16) and eosin

341   (Sigma, 318906). For immunostaining, 5 μm-thick paraffin sections were deparaffinized and autoclaved

342   in target retrieval solution (DAKO) for 10 min at 121 °C. Sections were blocked with Blocking One Histo

343   (Nacalai) for 30 min at room temperature and then incubated with primary antibodies as outlined below:

344   mouse anti-CHD4 (1:500, Abcam, ab70469), rabbit anti-DDX4 (1:500, Abcam, ab13840), goat anti-

345   CD117/c-kit (1:200, R&D, AF1356), rabbit anti-Cleaved Caspase-3 (1:200, Cell Signaling Technology,

346   #9661), rabbit anti-FOXO3 (1:200, Cell Signaling Technology, #2497) overnight at 4 °C. Sections were

347   washed with PBST (PBS containing 0.1% Tween 20) three times at room temperature for 5 min and then

348   incubated with the corresponding secondary (Invitrogen) at 1:500 dilution for 1 h at room temperature.

349   Finally, sections were counterstained with DAPI and mounted using 20 μL undiluted ProLong Gold

350   Antifade Mountant (ThermoFisher Scientific, P36930). Images were obtained by an all-in-one

351   fluorescence microscope (BZ-X810, KEYENCE) equipped with an optical sectioning module (BZ-H4XF,

352   KEYENCE).

353

354   **Quantification of ovarian follicles**

355   For counting the number of follicles, paraffin-embedded ovaries were serially sectioned at 5 μm

356   thickness, and all sections were mounted on slides. 5 μm-thick paraffin serially sections were

357   deparaffinized and stained with hematoxylin and eosin. Ovarian follicles at different developmental

358   stages, including primordial (type 1 and type 2) as non-growing oocytes, and primary (type 3) and pre-

359   antral (type 4 and type 5) as growing oocytes, were counted in every fifth section of the collected sections

360   from one ovary, based on the standards established method[56]. In each section, only those follicles in

361   which the nucleus of the oocyte was clearly visible were counted, and the cumulative follicle counts were

362   multiplied by a correction factor of 5 to represent the estimated number of follicles in an ovary.

363

364   **Meiotic chromosome spreads and immunofluorescence**

365   Chromosome spreads of oocytes from neonatal ovaries were prepared as described[7]. Briefly, ovaries were

366   digested in 200 μl TrypLE™ Express Enzyme (1X) supplemented with 0.3 mg/ml Collagenase Type 1

367   and 10 mg/ml DNase I and incubated at 37°C for 25 min with gentle agitation. After incubation, the

368   ovaries were dissociated by gentle pipetting using the Fisherbrand[TM] Premium Plus MultiFlex Gel-

369   Loading Tips until no visible tissue pieces. 2 ml DMEM/F-12 medium supplemented with 10% FBS was

370   added to the suspension to stop enzyme reaction. Cell suspension was incubated in hypotonic extraction

371   buffer [HEB: 30 mM Tris base, 17 mM trisodium citrate, 5 mM ethylenediaminetetraacetic acid (EDTA),

372   50 mM sucrose, 5 mM dithiothreitol (DTT), 1× cOmplete Protease Inhibitor Cocktail (Sigma,

373   11836145001), 1× phosphatase inhibitor cocktail 2 (Sigma, P5726-5ML), pH 8.2] on ice for 10 min.

374   30 μL of the suspension was applied to positively charged slides (Probe On Plus: Thermo Fisher

375   Scientific, 22-230-900); before application of the suspension, the slides had been incubated in chilled

376   fixation solution (2% paraformaldehyde, 0.1% Triton X-100, 0.02% sodium monododecyl sulfate,

377   adjusted to pH 9.2 with sodium borate buffer). The slides were placed in "humid chambers" overnight at

378   room temperature. Then, the slides were washed twice in 0.4% Photo-Flo 200 (Kodak, 146-4510), 2 min

379   per wash. Slides were dried completely at room temperature before staining or storage in slide boxes at

380   −80 °C.

381

382   **Flow cytometry and cell sorting**

383   Flow cytometric experiments and cell sorting were performed using SH800S (SONY), with antibody-

384   stained testicular single-cell suspensions prepared as described previously. Data were analyzed using

385   SH800S software (SONY) and FCS Express 7 (De Novo Software).

386

387   For ATAC-seq and CUT&Tag, P1 oocytes were collected using the *Stella*-GFP transgene. To prepare

388   single cells suspension for cell sorting, ovaries were digested in 200 μl TrypLE™ Express Enzyme (1X)

389   supplemented with 0.3 mg/ml Collagenase Type 1 and 10 mg/ml DNase I and incubated at 37°C for

390   25 min with gentle agitation. After incubation, the ovaries were dissociated by gentle pipetting using the

391   FisherbrandTM Premium Plus MultiFlex Gel-Loading Tips until no visible tissue pieces. 2 ml DMEM/F-

392   12 medium supplemented with 10% FBS was added to the suspension to stop enzyme reaction. Cells

393   were suspended in FACS buffer (PBS containing 2% FBS) and filtered into a 5 ml FACS tube through a

394   35 μm nylon mesh cap (Falcon, 352235). GFP[+] oocytes were collected after removing small and large

395   debris in FSC-A versus SSC-A gating and doublets in FSC-W versus FSC-H gating.

396

397   Collection of male germ cells was modified from described[57]. Briefly, to prepare single cells suspension

398   for cell sorting, detangled seminiferous tubules from P3 mouse testes were incubated in 1× Krebs-Ringer

399   Bicarbonate Buffer (Sigma, K4002) supplemented with 1.5 mg/ml Collagenase Type 1 and 0.04 mg/ml

400   DNase I at 37°C for 15 min with gentle agitation and dissociated using vigorous pipetting. Then add

401   0.75mg/ml Hyaluronidase (Sigma, H3506) and incubate at 37°C for 10 min with gentle agitation and

402   dissociated using vigorous pipetting.10 ml DMEM/F-12 medium supplemented with 10% FBS was added

403   to the suspension to stop enzyme reaction. The cell suspension was washed with 10 ml FACS buffer three

404   times by centrifugation at 300 × g for 5 min and filtered through a 70 μm nylon cell strainer (Falcon,

405   352350). The cell suspension was stained with cocktails of antibodies diluted with FACS buffer listed as

406   follows: PE-conjugated anti-mouse/human CD324 (E-Cadherin) antibody (1:500, Biolegend, 147303) and

407   FITC-conjugated anti-mouse CD9 antibody (1:500, Biolegend, 124808). After 50min incubation on ice,

408   cells were washed with 10 ml FACS buffer three times by centrifugation at 300 × g for 5 min and filtered

409   into a 5 ml FACS tube through a 35 μm nylon mesh cap. 7-AAD Viability Stain (Invitrogen, 00-6993-50)

410   and 0.01 mg/ml DNase I was added to cell suspension for the exclusion of dead cells. Samples were kept

411   on ice until sorting. Cells were analyzed after removing small and large debris in FSC-A versus SSC-A

412   gating, doublets in FSC-W versus FSC-H gating, and 7AAD^{+} dead cells. Then, the desired cell population

413   was collected in gates and determined based on antibody staining.

414

415   **RNA-seq library generation and sequencing**

416   RNA-seq libraries of oocytes from P1, P5, and P10 ovaries were prepared as described[7]; briefly, 500 non-

417   growing and 100 growing oocytes isolated from ovaries were pooled as one replicate, and two

418   independent biological replicates were used for RNA-seq library generation. Total RNA was extracted

419   using the RNeasy Plus Micro Kit (QIAGEN, Cat # 74034) according to the manufacturer's instructions.

420   Library preparation was performed with NEBNext® Single Cell/Low Input RNA Library Prep Kit for

421   Illumina® (NEB, E6420S) according to the manufacturer's instruction. Prepared RNA-seq libraries were

422   sequenced on the HiSeq X system (Illumina) with paired-ended 150-bp reads.

423

424   **ATAC-seq library generation and sequencing**

425   ATAC-seq libraries of germ cells were prepared as described[39]; briefly, 10,000 FACS-sorted cells were

426   isolated from P1 ovaries or P3 testis and pooled as one replicate, and two independent biological

427   replicates were used for ATAC-seq library generation. Samples were lysed in 50 μl of lysis buffer (10

428   mM Tris–HCl (pH 7.4), 10 mM NaCl, 3 mM MgCl$_2$, and 0.1% NP-40, 0.1% Tween-20, and 0.01%

429   Digitonin) on ice for 10 min. Immediately after lysis, the samples were spun at 500 × g for 10 min at 4 °C

430   and the supernatant removed. The sedimented nuclei were then incubated in 10 µl of transposition mix

431   (0.5 µl homemade Tn5 transposase (~1µg/µl), 5 µl 2× TD buffer (10 mM Tris–HCl (pH 7.6), 10 mM

432   MgCl$_2$, and 20% Dimethyl Formamide), 3.3 µl PBS, 0.1 µl 1% digitonin, 0.1 µl 10% Tween-20, and 1 µl

433   water) at 37 °C for 30 min in a thermomixer with shaking at 500 rpm. After tagmentation, the transposed

434   DNA was purified with a MinElute kit (Qiagen). Polymerase chain reaction (PCR) was performed to

435   amplify the library using the following conditions: 72 °C for 3 min; 98°C for 30 s; thermocycling at 98 °C

436   for 10 s, 60 °C for 30 s, and 72 °C for 1 min. qPCR was used to estimate the number of additional cycles

437   needed to generate products at 25% saturation. Seven to eight additional PCR cycles were added to the

438   initial set of five cycles. Amplified DNA was purified by SPRIselect bead (Beckman Coulter). ATAC-

439   seq libraries were sequenced on the HiSeq X ten system (Illumina) with 150-bp paired-end reads.

440

441   **CUT&Tag library generation and sequencing**

442   CUT&Tag libraries from P1 oocytes for CHD4 were generated as previously described[41, 58] (a step-by-

443   step protocol https://www.protocols.io/view/bench-top-cut-amp-tag-kqdg34qdpl25/v3) using

444   CUTANA™ pAG-Tn5 (Epicypher, 15-1017). Briefly, 10,000 FACS-sorted cells were isolated from P1

445   *Chd4 f/f* ovaries and pooled as one replicate and two independent biological replicates were used for

446   CUT&Tag library generation. The antibodies used were mouse anti-CHD4 (1:50, Abcam, ab70469) and

447   rabbit α-mouse antibody (1:100, Abcam, ab46540). CUT&Tag libraries were sequenced on the NovaSeq

448   X Plus system (Illumina) with 150-bp paired-end reads.

449

450   **RNA-seq data processing**

451   Raw paired-end RNA-seq reads after trimming by trimmomatic (version 0.39)[59] were aligned to the

452   mouse (GRCm38/mm10) genome using by STAR (version STAR_2.5.4b)[60] with default arguments. All

453   unmapped and non-uniquely mapped reads were filtered out by samtools (version 1.9)[61] before being

454   subjected to downstream analyses. To quantify aligned reads in RNA-seq, aligned read counts for each

455   gene were generated using featureCounts (v2.0.1), which is part of the Subread package [62] based on

456   annotated genes (GENCODE vM25). The TPM values of each gene were for comparative expression

457   analyses and computing the Pearson correlation coefficient between biological replicates using corrplot[63].

458   To detect differentially expressed genes between CHD4 Dctrl and CHD4 DcKO, or CHD4 Gctrl and

459   CHD4 GcKO, DESeq2 (version 1.42.1)[64] was used for differential gene expression analyses with cutoffs

460   ≥2-fold change and binominal tests (Padj < 0.05; P values were adjusted for multiple testing using the

461   Benjamini–Hochberg method). Padj values were used to determine significantly dysregulated genes.

462   To perform GO analyses, we used the online functional annotation clustering tool Metascape[65]

463   (http://metascape.org). Further analyses were performed with R and visualized as heatmaps using

464   Morpheus (https://software.broadinstitute.org/morpheus, Broad Institute).

465

466   **ATAC-seq and CUT&Tag data processing**

467   Raw paired-end ATAC-seq and CUT&Tag reads after trimming by Trim-galore

468   (https://github.com/FelixKrueger/TrimGalore) (version 0.6.7) were aligned to either the mouse

469   (GRCm38/mm10) genomes using bowtie2 (version 2.3.3.1)[66] with default arguments. The aligned reads

470   were filtered to remove alignments mapped to multiple locations by calling grep with the -v option before

471   being subjected to downstream analyses. PCR duplicates were removed using the 'MarkDuplicates'

472   command in Picard tools (version 2.23.8) (https://broadinstitute.github.io/picard/, Broad Institute). To

473   compare replicates, Pearson correlation coefficients were calculated and plotted by 'multiBamSummary

474   bins' and 'plot correlation' functions of deepTools (version 3.3.0)[67]. Biological replicates were pooled for

475   visualization and other analyses after validation of reproducibility. Peak calling for ATAC-seq and

476   CUT&Tag data was performed using MACS3 (version 3.0.0a7)[68] with default arguments. We computed

477   the number of overlapping peaks between peak files using BEDtools[69] (version 2.28.0) function intersect.

478   To detect genes adjacent to ATAC-seq and CUT&Tag peaks, we used the HOMER (version 4.9.1)[70]

479   function annotatePeaks.pl. The deeptools[67] was used to draw tag density plots and heatmaps for reads

480   enrichments. To visualize ATAC-seq and CUT&Tag data using the Integrative Genomics Viewer (Broad

481   Institute)[71], BPM normalized counts data were created from sorted BAM files using the deeptools[67]. To

482   perform functional annotation enrichment of CHD4, we used GREAT tools[72].

483

484   **Statistics**

485   Statistical methods and P values for each plot are listed in the figure legends and/or in the Methods. In

486   brief, all grouped data are represented as mean ± SD. All box-and-whisker plots are represented as center

487   lines (median), box limits (interquartile range; 25th and 75th percentiles), and whiskers (maximum value

488   not exceeding 1.5x the interquartile range (IQR) from the hinge) unless stated otherwise. Statistical

489   significance for pairwise comparisons was determined using two-sided Mann–Whitney U-tests and two-

490   tailed unpaired t-tests. Next-generation sequencing data (RNA-seq, ATAC-seq, and CUT&Tag) were

491   based on two independent replicates. No statistical methods were used to predetermine sample size in

492   these experiments. Experiments were not randomized, and investigators were not blinded to allocation

493   during experiments and outcome assessments.

494

495   **Data availability**

496   The raw data of quantifications presented in the main figures and supplementary figures are provided as

497   "Source data files". RNA-seq data reported in this study were deposited to the Gene Expression Omnibus

498   (accession no. GSE273309). Source data are provided with this paper.

499

500   **Code availability**

501   Source code for all software and tools used in this study with documentation, examples, and additional

502   information, is available at the URLs listed below.

503

504   trimmomatic [http://www.usadellab.org/cms/?page=trimmomatic]

505   STAR [https://github.com/alexdobin/STAR]

506   featureCounts [http://subread.sourceforge.net]

507   DESeq2 [https://bioconductor.org/packages/release/bioc/html/DESeq2.html]

508   corrplot [https://github.com/taiyun/corrplot]

509   ggplot2 [https://github.com/tidyverse/ggplot2]

510   Metascape [http://metascape.org]

511   Morpheus [https://software.broadinstitute.org/morpheus/]

512   Trim-galore [https://github.com/FelixKrueger/TrimGalore]

513   Bowtie2 [https://github.com/BenLangmead/bowtie2]

514   Picard [https://broadinstitute.github.io/picard/]

515   deepTools [https://github.com/deeptools/deepTools]

516   MACS3 [https://github.com/macs3-project/MACS]

517   Bedtools [https://github.com/arq5x/bedtools2]

518   HOMER [http://homer.ucsd.edu/homer/index.html]

519   GREAT [http://great.stanford.edu/public/html/]

520

References

1. Grive KJ, Freiman RN. The developmental origins of the mammalian ovarian reserve. *Development* **142**, 2554-2563 (2015).

2. Ford EA, Beckett EL, Roman SD, McLaughlin EA, Sutherland JM. Advances in human primordial follicle activation and premature ovarian insufficiency. *Reproduction* **159**, R15-r29 (2020).

3. Hancock GV, Wamaitha SE, Peretz L, Clark AT. Mammalian primordial germ cell specification. *Development* **148**, (2021).

4. Martínez-Marchal A*, et al.* The DNA damage response is required for oocyte cyst breakdown and follicle formation in mice. *PLoS Genet* **16**, e1009067 (2020).

5. Tharp ME, Malki S, Bortvin A. Maximizing the ovarian reserve in mice by evading LINE-1 genotoxicity. *Nat Commun* **11**, 330 (2020).

6. Niu W, Spradling AC. Mouse oocytes develop in cysts with the help of nurse cells. *Cell* **185**, 2576-2590.e2512 (2022).

7. Hu M*, et al.* PRC1-mediated epigenetic programming is required to generate the ovarian reserve. *Nat Commun* **13**, 4510 (2022).

8. Hu M, Schultz RM, Namekawa SH. Epigenetic programming in the ovarian reserve. *Bioessays* **45**, e2300069 (2023).

9. Soyal SM, Amleh A, Dean J. FIGalpha, a germ cell-specific transcription factor required for ovarian follicle formation. *Development* **127**, 4645-4654 (2000).

10. Trombly DJ, Woodruff TK, Mayo KE. Suppression of Notch signaling in the neonatal mouse ovary decreases primordial follicle formation. *Endocrinology* **150**, 1014-1024 (2009).

11. Patton BK, Madadi S, Pangas SA. Control of ovarian follicle development by TGFβ family signaling. *Curr Opin Endocr Metab Res* **18**, 102-110 (2021).

12. Niu W*, et al.* JNK signaling regulates E-cadherin junctions in germline cysts and determines primordial follicle formation in mice. *Development* **143**, 1778-1787 (2016).

13. Shimamoto S*, et al.* Hypoxia induces the dormant state in oocytes through expression of Foxo3. *Proc Natl Acad Sci U S A* **116**, 12321-12326 (2019).

14. Clapier CR, Iwasa J, Cairns BR, Peterson CL. Mechanisms of action and regulation of ATP-dependent chromatin-remodelling complexes. *Nat Rev Mol Cell Biol* **18**, 407-422 (2017).

15. Hota SK, Bruneau BG. ATP-dependent chromatin remodeling during mammalian development. *Development* **143**, 2882-2897 (2016).

16. Arends T*, et al.* CHD4 is essential for transcriptional repression and lineage progression in B lymphopoiesis. *Proc Natl Acad Sci U S A* **116**, 10927-10936 (2019).

17. Zhao H*, et al.* The chromatin remodeler Chd4 maintains embryonic stem cell identity by controlling pluripotency- and differentiation-associated genes. *J Biol Chem* **292**, 8507-8519 (2017).

18. O'Shaughnessy-Kirwan A, Signolet J, Costello I, Gharbi S, Hendrich B. Constraint of gene expression by the chromatin remodelling protein CHD4 facilitates lineage specification. *Development* **142**, 2586-2597 (2015).

19. Yoshida T*, et al.* Chromatin restriction by the nucleosome remodeler Mi-2β and functional interplay with lineage-specific transcription regulators control B-cell differentiation. *Genes Dev* **33**, 763-781 (2019).

20. Li P*, et al.* CHD4 acts as a critical regulator in the survival of spermatogonial stem cells in mice†. *Biol Reprod* **107**, 1331-1344 (2022).

21. de Castro RO, Carbajal A, Previato de Almeida L, Goitea V, Griffin CT, Pezza RJ. Mouse Chd4-NURD is required for neonatal spermatogonia survival and normal gonad development. *Epigenetics Chromatin* **15**, 16 (2022).

22. Cafe SL*, et al.* A regulatory role for CHD4 in maintenance of the spermatogonial stem cell pool. *Stem Cell Reports* **16**, 1555-1567 (2021).

23. Williams CJ*, et al.* The chromatin remodeler Mi-2beta is required for CD4 expression and T cell development. *Immunity* **20**, 719-733 (2004).

24. Gallardo T, Shirley L, John GB, Castrillon DH. Generation of a germ cell-specific mouse transgenic Cre line, Vasa-Cre. *Genesis* **45**, 413-417 (2007).

25. John GB, Gallardo TD, Shirley LJ, Castrillon DH. Foxo3 is a PI3K-dependent molecular switch controlling the initiation of oocyte growth. *Dev Biol* **321**, 197-204 (2008).

26. Soh YQ, Junker JP, Gill ME, Mueller JL, van Oudenaarden A, Page DC. A Gene Regulatory Program for Meiotic Prophase in the Fetal Ovary. *PLoS Genet* **11**, e1005531 (2015).

27. Romanienko PJ, Camerini-Otero RD. The mouse Spo11 gene is required for meiotic chromosome synapsis. *Mol Cell* **6**, 975-987 (2000).

28. Baudat F, Manova K, Yuen JP, Jasin M, Keeney S. Chromosome synapsis defects and sexually dimorphic meiotic progression in mice lacking Spo11. *Mol Cell* **6**, 989-998 (2000).

29. de Vries FA*, et al.* Mouse Sycp1 functions in synaptonemal complex assembly, meiotic recombination, and XY body formation. *Genes Dev* **19**, 1376-1389 (2005).

30. Shin YH*, et al.* Hormad1 mutation disrupts synaptonemal complex formation, recombination, and chromosome segregation in mammalian meiosis. *PLoS Genet* **6**, e1001190 (2010).

31. Daniel K*, et al.* Meiotic homologue alignment and its quality surveillance are controlled by mouse HORMAD1. *Nat Cell Biol* **13**, 599-610 (2011).

32. Kogo H, Tsutsumi M, Ohye T, Inagaki H, Abe T, Kurahashi H. HORMAD1-dependent checkpoint/surveillance mechanism eliminates asynaptic oocytes. *Genes Cells* **17**, 439-454 (2012).

33. Luo M*, et al.* MEIOB exhibits single-stranded DNA-binding and exonuclease activities and is essential for meiotic recombination. *Nat Commun* **4**, 2788 (2013).

34. Shibuya H, Hernández-Hernández A, Morimoto A, Negishi L, Höög C, Watanabe Y. MAJIN Links Telomeric DNA to the Nuclear Membrane by Exchanging Telomere Cap. *Cell* **163**, 1252-1266 (2015).

35. Kanehisa M, Goto S. KEGG: kyoto encyclopedia of genes and genomes. *Nucleic Acids Res* **28**, 27-30 (2000).

36. Goodman JV*, et al.* The chromatin remodeling enzyme Chd4 regulates genome architecture in the mouse brain. *Nat Commun* **11**, 3419 (2020).

37. Graca Marques J*, et al.* The Chromatin Remodeler CHD4 Sustains Ewing Sarcoma Cell Survival by Controlling Global Chromatin Architecture. *Cancer Res* **84**, 241-257 (2024).

38. Buenrostro JD, Giresi PG, Zaba LC, Chang HY, Greenleaf WJ. Transposition of native chromatin for fast and sensitive epigenomic profiling of open chromatin, DNA-binding proteins and nucleosome position. *Nat Methods* **10**, 1213-1218 (2013).

39. Corces MR*, et al.* An improved ATAC-seq protocol reduces background and enables interrogation of frozen tissues. *Nat Methods* **14**, 959-962 (2017).

40. Kojima ML, de Rooij DG, Page DC. Amplification of a broad transcriptional program by a common factor triggers the meiotic cell cycle in mice. *Elife* **8**, (2019).

41. Kaya-Okur HS*, et al.* CUT&Tag for efficient epigenomic profiling of small samples and single cells. *Nat Commun* **10**, 1930 (2019).

42. Lan ZJ, Xu X, Cooney AJ. Differential oocyte-specific expression of Cre recombinase activity in GDF-9-iCre, Zp3cre, and Msx2Cre transgenic mice. *Biol Reprod* **71**, 1469-1474 (2004).

43. Korsmeyer SJ, Wei MC, Saito M, Weiler S, Oh KJ, Schlesinger PH. Pro-apoptotic cascade activates BID, which oligomerizes BAK or BAX into pores that result in the release of cytochrome c. *Cell Death Differ* **7**, 1166-1173 (2000).

44. Yoshida S. Heterogeneous, dynamic, and stochastic nature of mammalian spermatogenic stem cells. *Curr Top Dev Biol* **135**, 245-285 (2019).

45. Nakagawa T*, et al.* A multistate stem cell dynamics maintains homeostasis in mouse spermatogenesis. *Cell Rep* **37**, 109875 (2021).

46. Hu M, Yeh YH, Maezawa S, Nakagawa T, Yoshida S, Namekawa SH. PRC1 directs PRC2-H3K27me3 deposition to shield adult spermatogonial stem cells from differentiation. *Nucleic Acids Res* **52**, 2306-2322 (2024).

47. Nashun B, *et al.* Continuous Histone Replacement by Hira Is Essential for Normal Transcriptional Regulation and De Novo DNA Methylation during Mouse Oogenesis. *Mol Cell* **60**, 611-625 (2015).

48. Ruth KS, *et al.* Genetic insights into biological mechanisms governing human ovarian ageing. *Nature* **596**, 393-397 (2021).

49. O'Shaughnessy A, Hendrich B. CHD4 in the DNA-damage response and cell cycle progression: not so NuRDy now. *Biochem Soc Trans* **41**, 777-782 (2013).

50. Broering TJ, Wang YL, Pandey RN, Hegde RS, Wang SC, Namekawa SH. BAZ1B is dispensable for H2AX phosphorylation on Tyrosine 142 during spermatogenesis. *Biol Open* **4**, 873-884 (2015).

51. Kim TW, *et al.* Ctbp2 Modulates NuRD-Mediated Deacetylation of H3K27 and Facilitates PRC2-Mediated H3K27me3 in Active Embryonic Stem Cell Genes During Exit from Pluripotency. *Stem Cells* **33**, 2442-2455 (2015).

52. Maezawa S, Yukawa M, Alavattam KG, Barski A, Namekawa SH. Dynamic reorganization of open chromatin underlies diverse transcriptomes during spermatogenesis. *Nucleic Acids Res* **46**, 593-608 (2018).

53. Kitamura Y, Namekawa SH. Epigenetic priming in the male germline. *Curr Opin Genet Dev* **86**, 102190 (2024).

54. Kato Y, *et al.* ELAVL2-directed RNA regulatory network drives the formation of quiescent primordial follicles. *EMBO Rep* **20**, e48251 (2019).

55. Payer B, Chuva de Sousa Lopes SM, Barton SC, Lee C, Saitou M, Surani MA. Generation of stella-GFP transgenic mice: a novel tool to study germ cell development. *Genesis* **44**, 75-83 (2006).

56. Pedersen T, Peters H. Proposal for a classification of oocytes and follicles in the mouse ovary. *J Reprod Fertil* **17**, 555-557 (1968).

57. Yeh YH, *et al.* Isolation of Murine Spermatogenic Cells using a Violet-Excited Cell-Permeable DNA Binding Dye. *J Vis Exp*, (2021).

58. Kaya-Okur HS, Janssens DH, Henikoff JG, Ahmad K, Henikoff S. Efficient low-cost chromatin profiling with CUT&Tag. *Nat Protoc* **15**, 3264-3283 (2020).

59. Bolger AM, Lohse M, Usadel B. Trimmomatic: a flexible trimmer for Illumina sequence data. *Bioinformatics* **30**, 2114-2120 (2014).

60. Dobin A, *et al.* STAR: ultrafast universal RNA-seq aligner. *Bioinformatics* **29**, 15-21 (2013).

61. Li H, *et al.* The Sequence Alignment/Map format and SAMtools. *Bioinformatics* **25**, 2078-2079 (2009).

62. Liao Y, Smyth GK, Shi W. featureCounts: an efficient general purpose program for assigning sequence reads to genomic features. *Bioinformatics* **30**, 923-930 (2014).

63. Michael F. Corrgrams. *The American Statistician* **56**, 316--324 (2002).

64. Love MI, Huber W, Anders S. Moderated estimation of fold change and dispersion for RNA-seq data with DESeq2. *Genome Biol* **15**, 550 (2014).

65. Zhou Y*, et al.* Metascape provides a biologist-oriented resource for the analysis of systems-level datasets. *Nat Commun* **10**, 1523 (2019).

66. Langmead B, Salzberg SL. Fast gapped-read alignment with Bowtie 2. *Nat Methods* **9**, 357-359 (2012).

67. Ramírez F*, et al.* deepTools2: a next generation web server for deep-sequencing data analysis. *Nucleic Acids Res* **44**, W160-165 (2016).

68. Zhang Y*, et al.* Model-based analysis of ChIP-Seq (MACS). *Genome Biol* **9**, R137 (2008).

69. Quinlan AR, Hall IM. BEDTools: a flexible suite of utilities for comparing genomic features. *Bioinformatics* **26**, 841-842 (2010).

70. Heinz S*, et al.* Simple combinations of lineage-determining transcription factors prime cis-regulatory elements required for macrophage and B cell identities. *Mol Cell* **38**, 576-589 (2010).

71. Robinson JT*, et al.* Integrative genomics viewer. In: *Nat Biotechnol*) (2011).

72. McLean CY*, et al.* GREAT improves functional interpretation of cis-regulatory regions. *Nat Biotechnol* **28**, 495-501 (2010).

Author information

Affiliations

Department of Microbiology and Molecular Genetics, University of California, Davis, California, 95616, USA

Yasuhisa Munakata, Mengwen Hu, Yuka Kitamura, Adam L. Bynder, Amelia S. Fritz, Richard M. Schultz & Satoshi H. Namekawa

Department of Biology, University of Pennsylvania, Philadelphia, PA 19104, USA

Richard M. Schultz

Contributions

Y.M. and S.H.N. designed the study. Y.M., M.H., Y.K., A.L.B., and A.S.F. performed experiments and analyzed the data. Y.M., M.H., Y.K., R.M.S., and S.H.N. interpreted the results. Y.M., R.M.S., and S.H.N wrote the manuscript with critical feedback from M.H., Y.K. R.M.S., and S.H.N. supervised the project.

Corresponding authors

Correspondence to Satoshi H. Namekawa and Richard M. Schultz

Ethics declarations

Competing Interests

The authors declare no competing interests.

Figure Legends

Fig 1. CHD4 deficiency causes oocyte loss.

a. Heatmap showing bulk RNA-seq gene expression (log2 (TPM+1) values) for core subunits of ATP-dependent remodeling complexes in oocytes during oogenesis. Embryonic day (E) 18.5 to postnatal day (P) 3 indicate oocytes with meiosis in progress. P4 and P6 small indicate oocytes residing in primordial follicles. P4 and P6-large indicate growing oocytes in primary follicles.

b. Schematic for mouse models and experiments.

c. Immunostaining of DDX4 (red) and CHD4 (green) in ovaries of *Chd4* Dctrl and *Chd4* DcKO at P1. CHD4 is present only in somatic cells in *Chd4* DcKO. Bars: 100 μm (20 μm in the boxed area). Yellow arrowheads indicate oocytes with no CHD4 expression.

d. Quantitative analysis of immunostaining. Percentages representing numbers of oocytes with CHD4 at P1. Data are presented as mean values ± SD. *** $P < 0.001$: Two-tailed unpaired t-tests. Three independent biological replicates were analyzed for each genotype.

e. Ovarian sections of *Chd4* Dctrl and *Chd4* DcKO mice at P1 and P5, respectively. The sections were stained with hematoxylin and eosin or immunostained for DDX4 (red). Bars: 100 μm. Three mice were analyzed for each genotype at each time point, and representative images are shown.

f. Dot plots showing the estimated numbers of oocytes per ovary from *Chd4* Dctrl and *Chd4* DcKO mice at P1 and P5, respectively. At least three mice were analyzed for each genotype at each time point. Central bars represent mean values. *** $P < 0.001$: ns, not significant; Two-tailed unpaired t-tests.

Fig 2. CHD4 is required for ovarian reserve formation.

a. Immunofluorescence staining of cKIT (white) and Cleaved Caspase-3 (red) in ovaries of *Chd4* Dctrl and *Chd4* DcKO at P1 and P3, respectively. Yellow arrowheads indicate Cleaved Caspase-3$^+$ apoptotic oocytes. Bars: 100 μm. Three mice were analyzed for each genotype at each time point, and representative images are shown.

b. Quantitative analysis of immunostaining. Dot plots showing the percentages of Cleaved Caspase-3$^+$ apoptotic oocytes per cKIT$^+$ oocytes at P1 and P3. Four independent biological replicates were analyzed for each genotype at each time point. ** $P < 0.01$: ns, not significant; Two-tailed unpaired t-tests.

c. Immunofluorescence staining of FOXO3 (red) and cKIT (green) in ovaries of *Chd4* Dctrl and *Chd4* DcKO at P1 and P5, respectively. Bars: 100 μm (50 μm in the boxed area). Three and five mice were analyzed for each genotype at each time point, and representative images are shown.

d. Quantitative analysis of immunostaining. Dot plots showing the percentages of nuclear FOXO3$^+$ oocytes per cKIT$^+$ oocytes at P1 and P5, respectively. Three and five independent biological replicates

816   were analyzed for each genotype at each time point. *** $P < 0.001$; ns, not significant; Two-tailed

817   unpaired t-tests.

818

819   **Fig 3. CHD4 represses meiotic prophase I genes and apoptosis-related genes.**

820   **a**. Comparison of transcriptomes between *Chd4* Dctrl and *Chd4* DcKO oocytes at P1 and P5,

821   respectively. 500 non-growing oocytes (NGOs) isolated from P1 or P5 ovaries were pooled as one

822   replicate, and two independent biological replicates were examined for RNA-seq. Differentially expressed

823   genes (DEGs: Log2FoldChange > 1, Padj < 0.05, binominal test with Benjamini–Hochberg correction) are

824   colored (red: upregulated in *Chd4* DcKO oocytes; blue: downregulated in *Chd4* DcKO oocytes).

825   **b**. Gene ontology term enrichments analysis of differentially expressed genes detected in **a**.

826   **c**. Violin plots with a Box plot indicate TPM values for female MPI-specific genes (104 genes) in *Chd4*

827   Dctrl and *Chd4* DcKO oocytes at P1 and P5. The central lines represent medians. The upper and lower

828   hinges correspond to the 25th and 75th percentiles. The upper and lower whiskers are extended from the

829   hinge to the largest value no further than the 1.5x inter-quartile range (IQR) from the hinge. * $P < 0.05$:

830   ns, not significant; Wilcoxon rank sum test.

831   **d**. Heatmaps showing expression of the P5 up-regulated differentially expressed MPI-specific genes in

832   *Chd4* DcKO oocytes at P1 and P5, respectively.

833   **e**. RNA-seq track views at the *Casp7* gene locus. The y-axis represents normalized tag counts for bulk

834   RNA-seq in each sample. Data ranges are shown in brackets.

835

836   **Fig 4. CHD4-dependent regulation of accessible chromatin in perinatal oocytes.**

837   **a**. Venn diagram indicates overlap of ATAC-seq peaks between *Chd4* Dctrl and *Chd4* DcKO oocytes at

838   P1.

839   **b**. Numbers and genomic distribution of ATAC-seq peaks in **a**.

840   **c**, **d**. Violin plots with a box plot indicate changes in TPM values of genes adjacent to specific ATAC-seq

841   peaks in *Chd4* Dctrl (**c**) and *Chd4* DcKO (**d**) oocytes at P1. The central lines represent medians. The

842   upper and lower hinges correspond to the 25th and 75th percentiles. The upper and lower whiskera are

843   extended from the hinge to the largest value no further than the 1.5x inter-quartile range (IQR) from the

844   hinge. *** $P < 0.001$; ** $P < 0.01$; ns, not significant; Wilcoxon rank sum test.

845   **e, f, g, h**. Heatmaps and average tag density plots of ATAC-seq enrichment around TSS (±2.5 kb) of

846   downregulated in *Chd4* DcKO oocytes at P1 (**e**) and P5 (**f**) and upregulated in *Chd4* DcKO oocytes at P1

847   (**g**) and P5 (**h**). *** $P < 0.001$; Wilcoxon rank sum test.

848 **i**. Representative track views of *Casp7* and *Stra8* gene loci show ATAC-seq signals in *Chd4* Dctrl and

849 *Chd4* DcKO oocytes at P1. The y-axis represents normalized tag counts for ATAC-seq in each sample.

850 The regions around TSSs are highlighted in red.

851

852 **Fig 5. CHD4 binding sites in non-growing oocytes at P1.**

853 **a**. Numbers and genomic distribution of CHD4 CUT&Tag peaks in *Chd4* f/f oocytes at P1.

854 **b**. Bar chart depicts the regional distribution of CHD4 CUT&Tag peaks to TSSs.

855 **c**. Overlap between ATAC distal peaks (> 1kb from TSSs) and CHD4 CUT&Tag peaks within classified

856 ATAC peaks.

857 **d**. Violin plots with a box plot indicate changes in TPM values of genes adjacent to CHD4 CUT&Tag

858 peaks in *Chd4* Dctrl and *Chd4* DcKO oocytes at P1 and P5. The central lines represent medians. The

859 upper and lower hinges correspond to the 25th and 75th percentiles. The upper and lower whiskers are

860 extended from the hinge to the largest value no further than the 1.5x inter-quartile range (IQR) from the

861 hinge. *** $P < 0.001$; ns, not significant; Wilcoxon rank sum test.

862 **e**. Heatmaps and average tag density plots of CHD4 enrichment around TSS (±2.5 kb) of DEG in *Chd4*

863 Dctrl and *Chd4* DcKO oocytes at P1 and P5. *** $P < 0.001$; Wilcoxon rank sum test.

864 **f, g**. Violin plots with a box plot indicate CHD4 enrichment around TSS (±1 kb) for female MPI-specific

865 genes (**f**, 104 genes) and apoptosis pathway genes in the KEGG database (**g**, 136 genes) in *Chd4* Dctrl and

866 *Chd4* DcKO oocytes at P1 and P5. The central lines represent medians. The upper and lower hinges

867 correspond to the 25th and 75th percentiles. The upper and lower whiskers are extended from the hinge to

868 the largest value no further than the 1.5x IQR from the hinge. *** $P < 0.001$; Wilcoxon rank sum test.

869 **h**. Representative track views of *Stra8* and *Bbc3* loci in P1 and P5 oocytes of indicated genotypes. Data

870 ranges are shown in brackets. Specific ATAC-seq peak regions in *Chd4* DcKO are highlighted.

871

872 **Fig 6. CHD4 is required for ovarian reserve maintenance.**

873 **a**. Schematic for mouse models and experiments.

874 **b**. Ovarian sections of *Chd4* Gctrl and *Chd4* GcKO mice at P10. The sections were stained with

875 hematoxylin and eosin or immunostained for DDX4 (red). Bars: 100 μm. Three mice were analyzed for

876 each genotype at each time point, and representative images are shown.

877 **c**. Dot plots showing the estimated numbers of oocytes per ovary from *Chd4* Gctrl and *Chd4* GcKO mice

878 at P10. At least three mice were analyzed for each genotype at each time point. Central bars represent

879 mean values. *** $P < 0.001$; * $P < 0.05$; Two-tailed unpaired t-tests.

880 **d**. Comparison of transcriptomes between *Chd4* Gctrl and *Chd4* GcKO non-growing oocytes (NGOs) and

881 growing oocytes (GOs) at P10. 500 NGOs and 100 GOs were isolated from P10 ovaries and were pooled

882   as one replicate, and two independent biological replicates were examined for RNA-seq. Differentially

883   expressed genes (DEGs: Log2FoldChange > 1, Padj < 0.05, binominal test with Benjamini–Hochberg

884   correction) are colored (red: upregulated in *Chd4* GcKO oocytes; blue: downregulated in *Chd4* GcKO

885   oocytes).

886   **e**. Violin plots with a Box plot indicate TPM values for female MPI-specific genes (104 genes) in *Chd4*

887   Gctrl and *Chd4* GcKO oocytes at P10. The central lines represent medians. The upper and lower hinges

888   correspond to the 25th and 75th percentiles. The upper and lower whiskers are extended from the hinge to

889   the largest value no further than the 1.5x inter-quartile range (IQR) from the hinge. ** $P < 0.01$; ns, not

890   significant; Wilcoxon rank sum test.

891   **f**. Track views showing RNA-seq signals in *Chd4* Gctrl and *Chd4* GcKO oocytes at P10, on *Stra8* and *Bid*

892   loci. The y-axis represents normalized tag counts for bulk RNA-seq in each sample. Data ranges are

893   shown in brackets.

894

895   **Fig 7. CHD4 suppresses pro-apoptotic genes for male germ cell survival, and summary model**.

896   **a**. Schematic for mouse models and experiments.

897   **b**. Immunostaining of DDX4 (red) in testicular sections in *Chd4* Dctrl and *Chd4* DcKO at P3. Bars: 100

898   μm. Three mice were analyzed for each genotype at each time point, and representative images are

899   shown.

900   **c**. Comparison of transcriptomes between *Chd4* Dctrl and *Chd4* DcKO undifferentiated male germ cells at

901   P3. Two independent biological replicates were examined for RNA-seq. Differentially expressed genes

902   (DEGs: Log2FoldChange > 1, Padj < 0.05, binominal test with Benjamini–Hochberg correction) are

903   colored (red: upregulated in *Chd4* DcKO undifferentiated male germ cells; blue: downregulated in *Chd4*

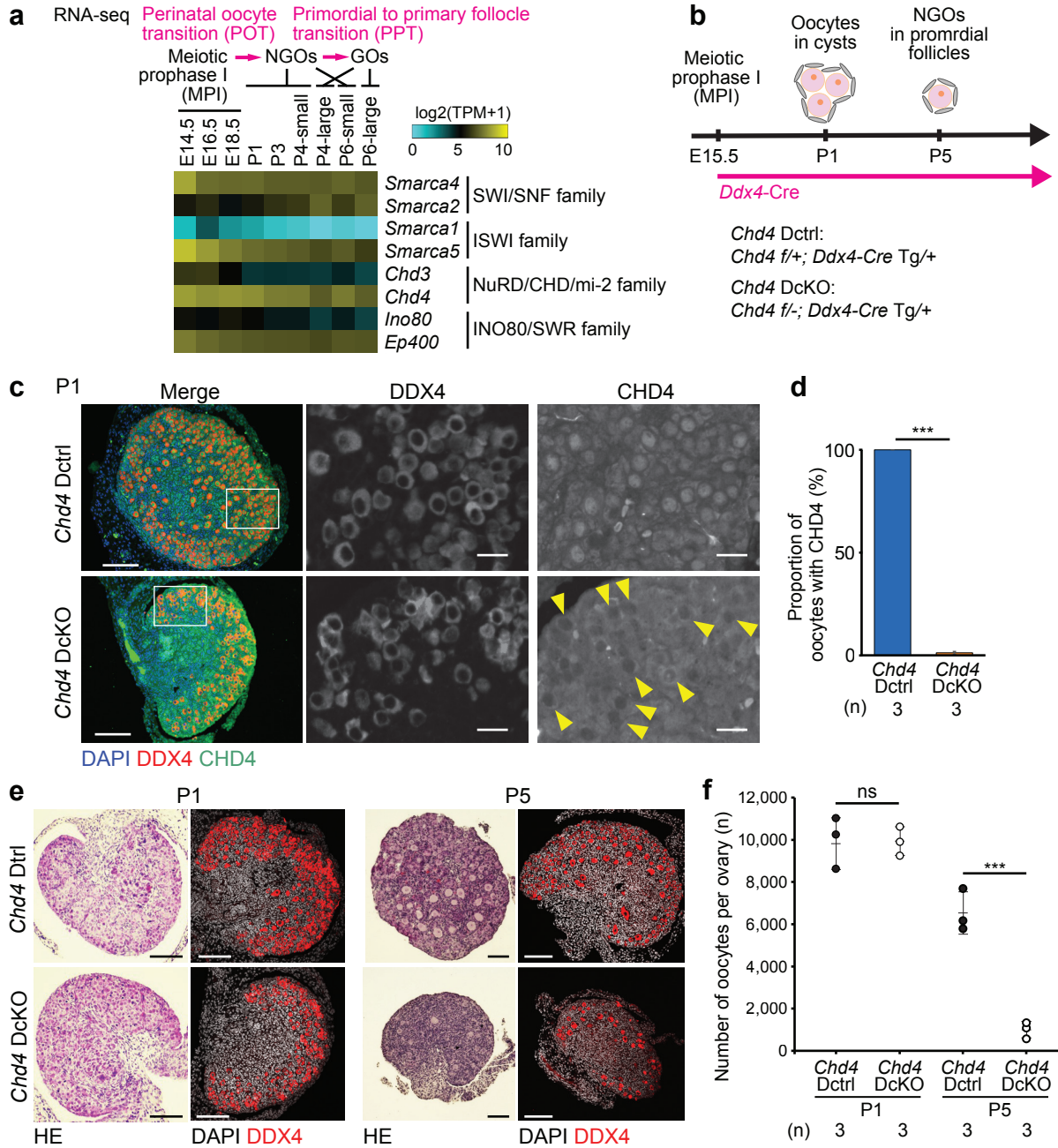904   DcKO undifferentiated male germ cells).

905   **d**. Representative track views of *Bbc3* locus in P3 undifferentiated male germ cells of indicated

906   genotypes. Data ranges are shown in brackets. Specific ATAC-seq peak regions in *Chd4* DcKO are

907   highlighted.

908   **e**. Venn diagram indicates overlap of ATAC-seq peaks between *Chd4* Dctrl and *Chd4* DcKO

909   undifferentiated male germ cells at P3.

910   **f**. Numbers and genomic distribution of ATAC-seq peaks in **e**.

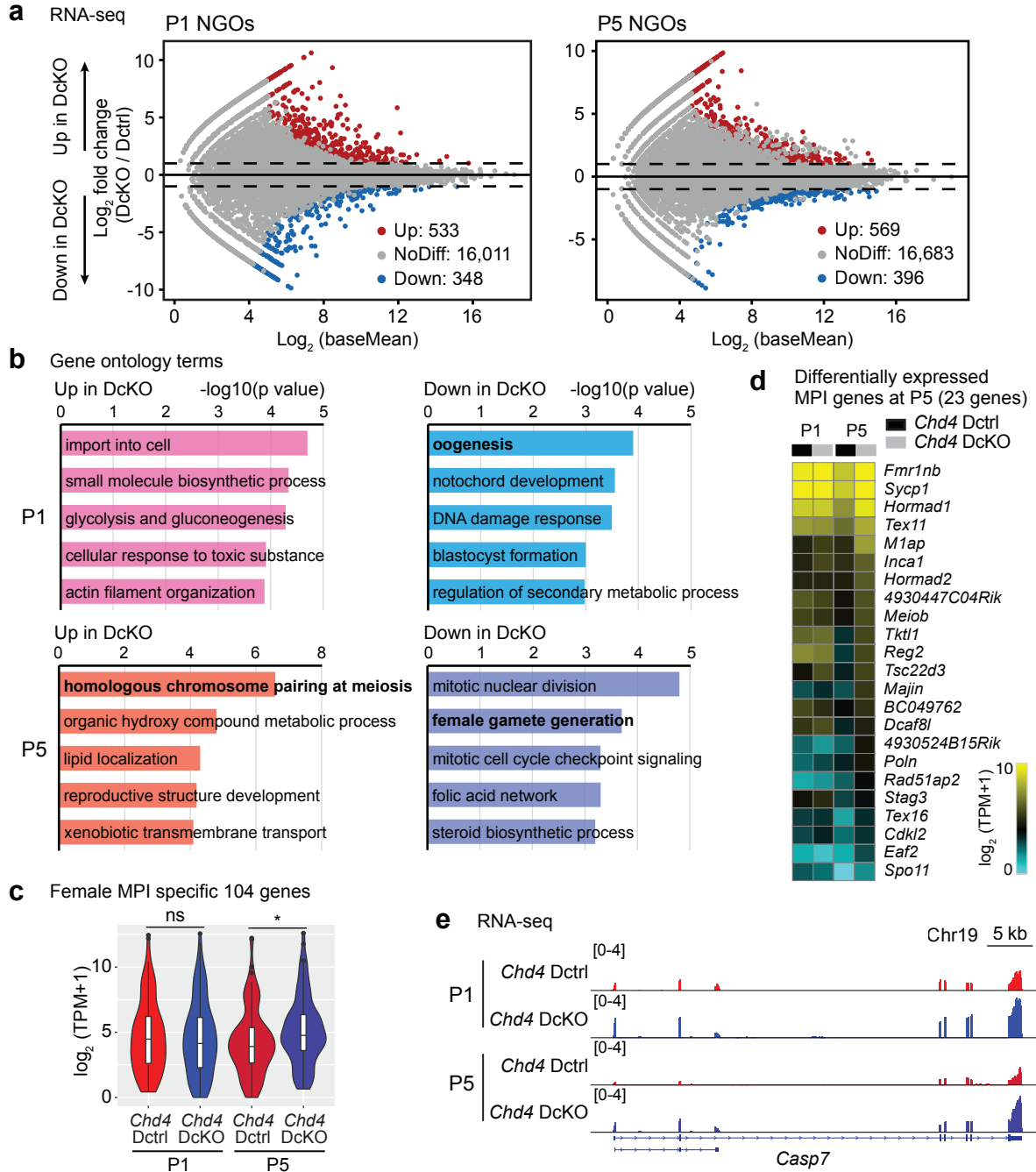911   **g**. Model of CHD4's function in oocytes and undifferentiated male germ cells.

Munakata_Figure 1

Munakata_Figure 2
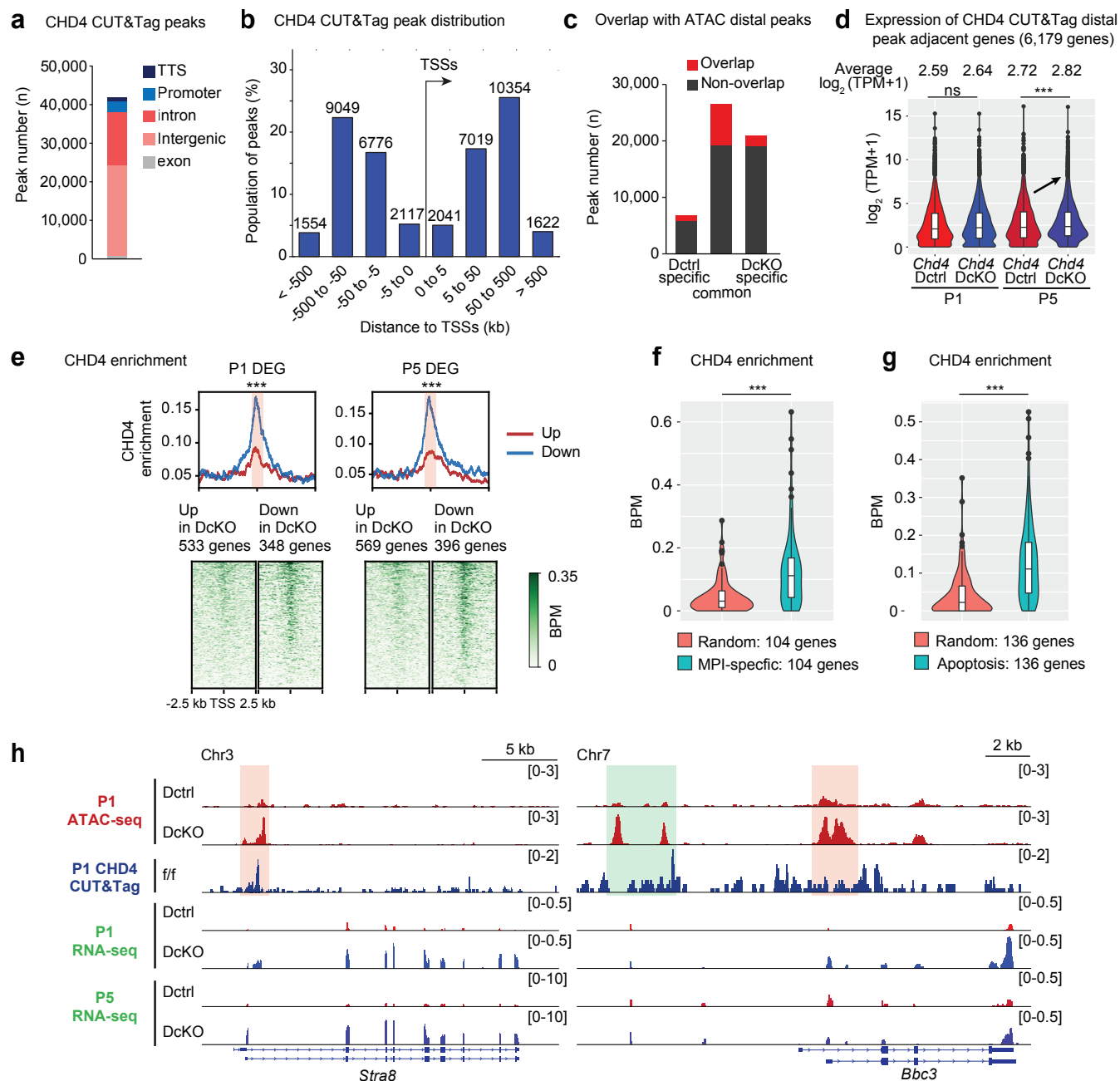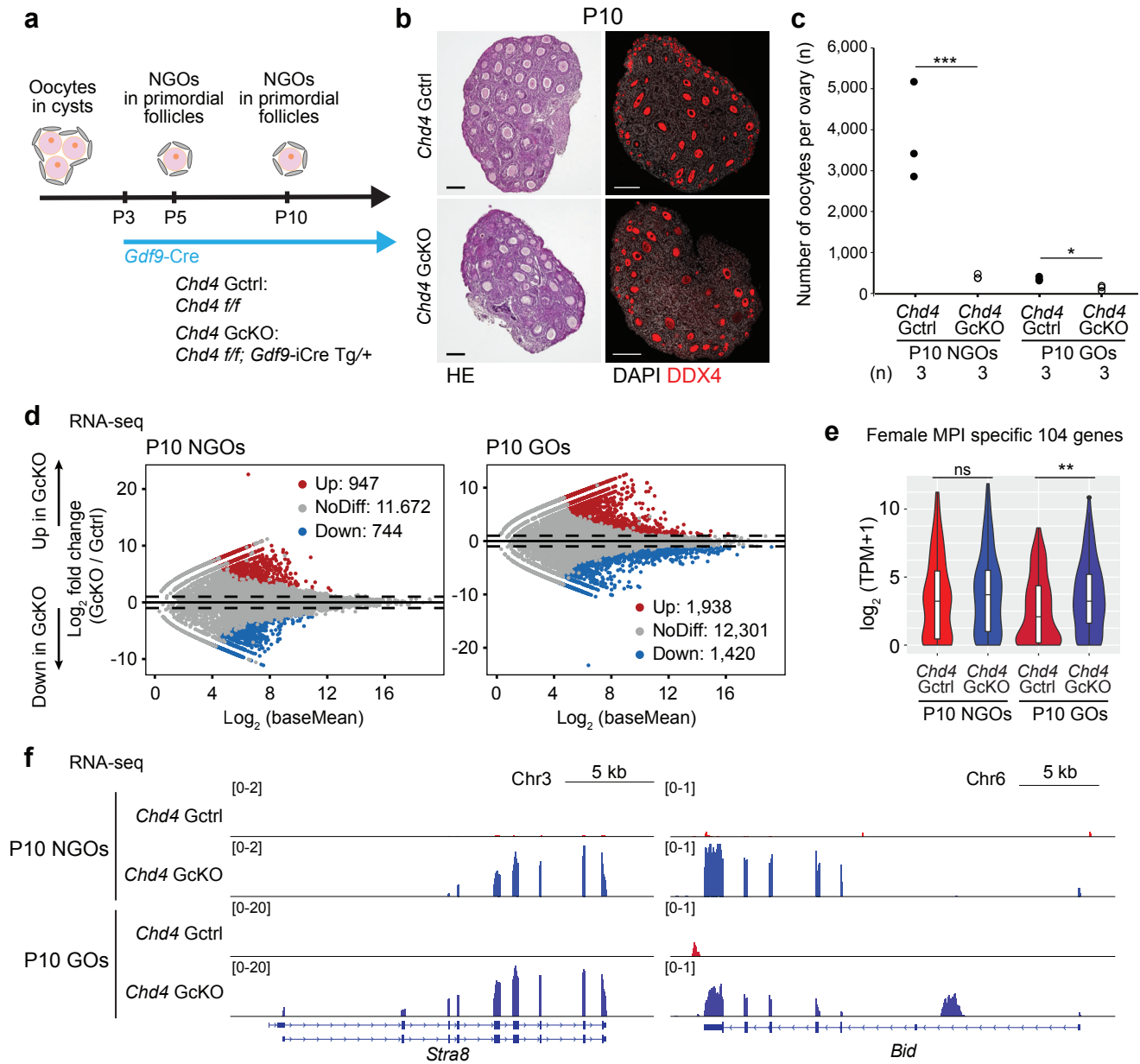
Munakata_Figure 3

a RNA-seq

b Gene ontology terms

c Female MPI specific 104 genes

d Differentially expressed MPI genes at P5 (23 genes)

e RNA-seq
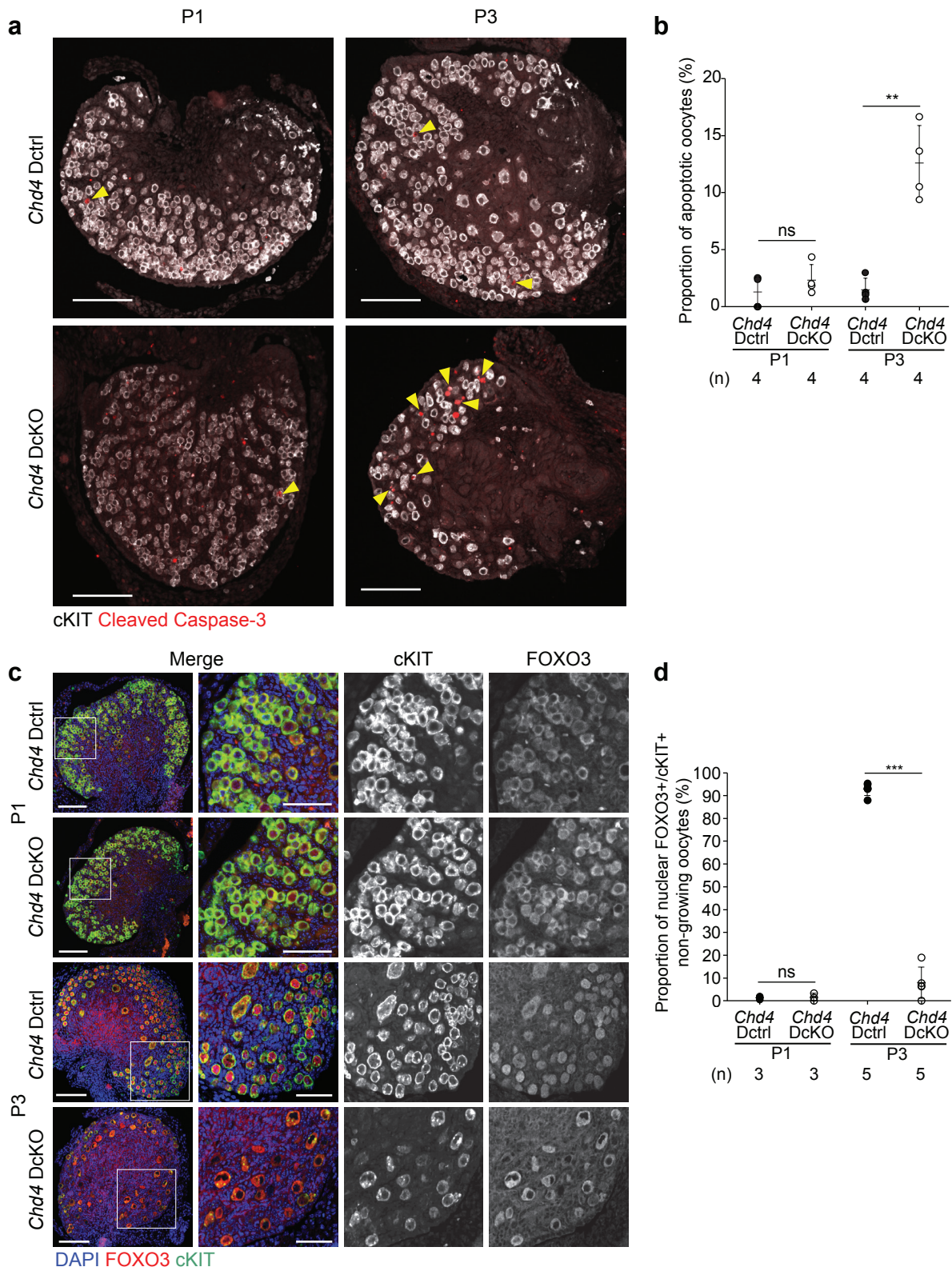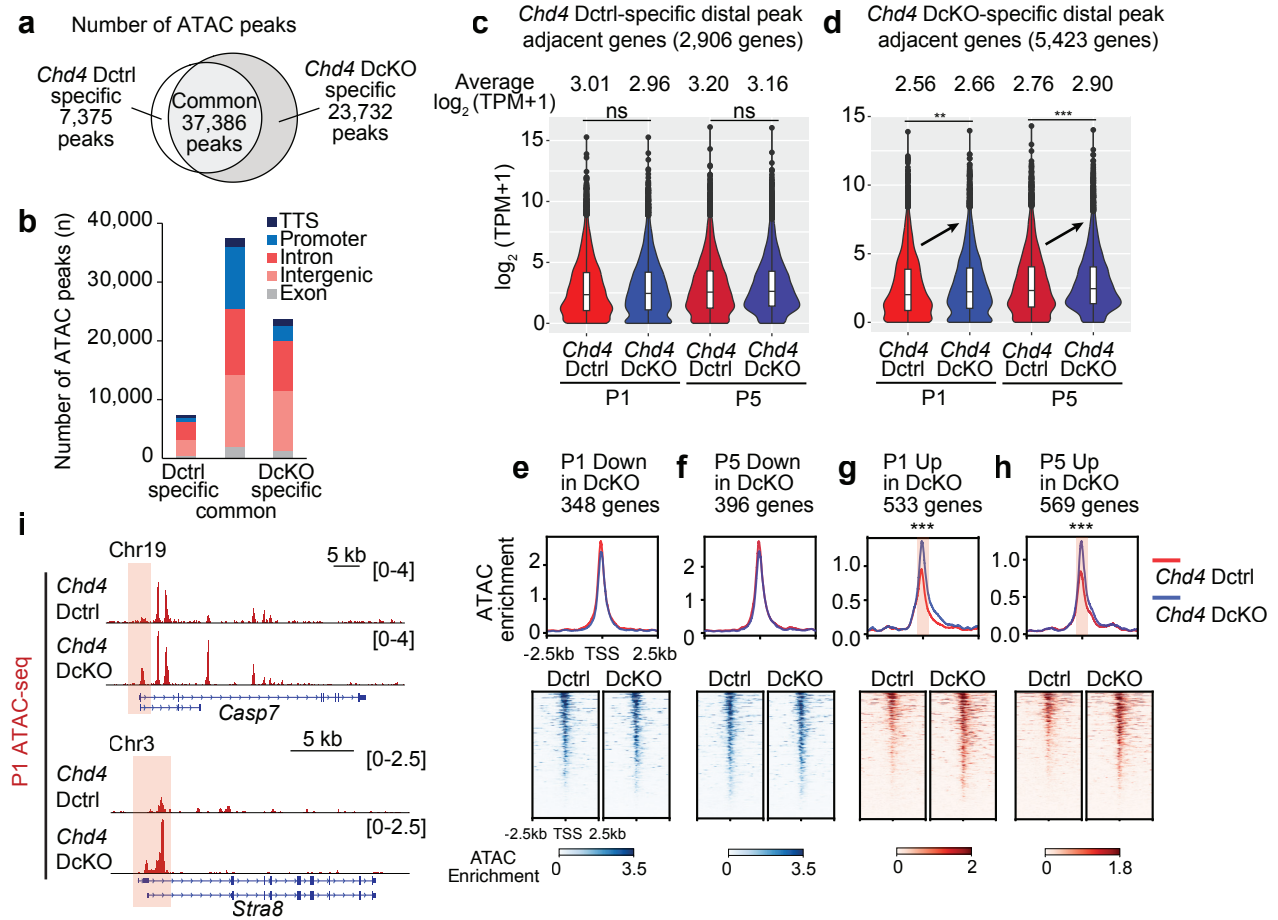
Munakata_Figure 4

Munakata_Figure 5

Munakata_Figure 6

a Male germ cells

E15.5   P3

Ddx4-Cre

Chd4 Dctrl:
Chd4 f/+; Ddx4-Cre Tg/+

Chd4 DcKO:
Chd4 f/-; Ddx4-Cre Tg/+

b P3

Chd4 Dtrl
Chd4 DcKO

DAPI DDX4

c RNA-seq

P3 Male germ cells
- Up: 696
- NoDiff: 20,729
- Down: 168

Up in DcKO / Down in DcKO
Log_2 fold change (DcKO / Dctrl)
Log_2 (baseMean)

d

Chr7 2 kb

P3 ATAC-seq
Chd4 Dctrl [0-4]
Chd4 DcKO [0-4]

P3 RNA-seq
Chd4 Dctrl [0-0.7]
Chd4 DcKO [0-0.7]

Bbc3

e Number of ATAC peaks

Chd4 Dctrl specific 3,109 peaks

Common 22,122 peaks

Chd4 DcKO specific 18,402 peaks

f

Number of ATAC peaks (n)

- TTS
- Promoter
- Intron
- Intergenic
- Exon

25,000
20,000
15,000
10,000
5,000
0

Dctrl specific common   DcKO specific

g

| WT oocytes Closed chromatin | CHD4-deficient oocytes Open chromatin | WT male germ cells Closed chromatin | CHD4-deficient male germ cells Open chromatin |

CHD4 | CHD4 | CHD4 | CHD4

Transcriptional repression MPI genes Apoptosis-related genes
Transcriptional derepression MPI genes Apoptosis-related genes
Transcriptional repression Apoptosis-related genes
Transcriptional derepression Apoptosis-related genes

↓

Ovarian reserve formation and maintenance Oocyte survival

Failure to form and maintain the ovarian reserve Oocyte loss

Male germ cell survival

Male germ cell loss